MOLECULAR AND CELLULAR BIOLOGY, July 2004, p. 6288–6297 Vol. 24, No. 14
0270-7306/04/$08.00+0 DOI: 10.1128/MCB.24.14.6288–6297.2004

Protein Profiling of Mouse Livers with Peroxisome Proliferator-Activated Receptor α Activation

Ruiyin Chu,[1]* Hanjo Lim,[1] Laura Brumfield,[1] Hong Liu,[2] Chris Herring,[1] Peter Ulintz,[3] Janardan K. Reddy,[4]* and Matthew Davison[1]

Departments of Functional Genomics,[1] Immunology Platform,[2] and Lead Generation Informatics,[3] Aventis Pharmaceuticals, Inc., Bridgewater, New Jersey 08807, and Department of Pathology, Feinberg School of Medicine, Northwestern University, Chicago, Illinois 60611[4]

Received 26 February 2004/Returned for modification 8 April 2004/Accepted 21 April 2004

Peroxisome proliferator-activated receptor α (PPARα) is important in the induction of cell-specific pleiotropic responses, including the development of liver tumors, when it is chronically activated by structurally diverse synthetic ligands such as Wy-14,643 or by unmetabolized endogenous ligands resulting from the disruption of the gene encoding acyl coenzyme A (CoA) oxidase (AOX). Alterations in gene expression patterns in livers with PPARα activation were delineated by using a proteomic approach to analyze liver proteins of Wy-14,643-treated and AOX$^{-/-}$ mice. We identified 46 differentially expressed proteins in mouse livers with PPARα activation. Up-regulated proteins, including acetyl-CoA acetyltransferase, farnesyl pyrophosphate synthase, and carnitine *O*-octanoyltransferase, are involved in fatty acid metabolism, whereas down-regulated proteins, including ketohexokinase, formiminotransferase-cyclodeaminase, fructose-bisphosphatase aldolase B, sarcosine dehydrogenase, and cysteine sulfinic acid decarboxylase, are involved in carbohydrate and amino acid metabolism. Among stress response and xenobiotic metabolism proteins, selenium-binding protein 2 and catalase showed a dramatic ~18-fold decrease in expression and a modest ~6-fold increase in expression, respectively. In addition, glycine *N*-methyltransferase, pyrophosphate phosphohydrolase, and protein phosphatase 1D were down-regulated with PPARα activation. These observations establish proteomic profiles reflecting a common and predictable pattern of differential protein expression in livers with PPARα activation. We conclude that livers with PPARα activation are transcriptionally geared towards fatty acid combustion.

Peroxisome proliferators constitute a group of chemicals with many applications in health and industry (16, 39–42). Administration of peroxisome proliferators to rodents results in marked hepatomegaly that is characterized by increased expression of the enzymes involved in fatty acid metabolism, proliferation of peroxisomes in hepatic parenchymal cells, and increased liver cell proliferation during the early stages (38–40). Chronic exposure to peroxisome proliferators leads to the development of hepatocellular carcinomas in rats and mice due to nongenotoxic mechanisms (16, 39, 41). The effects of peroxisome proliferators in rodents are mediated by peroxisome proliferator-activated receptor α (PPARα), a member of the group of transcription factors that regulates the expression of genes involved in lipid metabolism and adipocyte differentiation (8, 20, 21). Activation of PPARα in rodent liver promotes expression of peroxisomal fatty acid β-oxidation system enzymes, including the first and rate-limiting enzyme acyl coenzyme A (acyl-CoA) oxidase (AOX) (18, 44). Mice deficient in AOX (AOX$^{-/-}$ mice) initially exhibit extensive microvesicular fatty metamorphosis of liver parenchymal cells as well as inflammatory reactions, and go on to develop regenerative hepatocytes that display massive spontaneous peroxisome proliferation (10, 11). Subsequently, liver tumors develop in AOX$^{-/-}$ mice by 15 months of age, similar to the result of sustained induction of PPARα in wild-type mice and rats by exogenous peroxisome proliferators (11). The deletion of AOX leads to the accumulation of unmetabolized AOX substrates, which serve as endogenous ligands responsible for the transcriptional activation of PPARα in vivo (10, 11, 18). Thus, the AOX$^{-/-}$ mouse is an ideal model for elucidating the connection between peroxisome proliferation and hepatocarcinogenesis without the need for using exogenous peroxisome proliferators. Furthermore, AOX$^{-/-}$ mice, in which PPARα is activated by natural or biological ligands, serve as a valuable model system for comparing changes in gene expression that manifest in wild-type mice following activation of PPARα by synthetic ligands.

Previously, 40 protein mass peaks identified by using the surface-enhanced laser desorption-ionization ProteinChip biology system were found to have twofold-higher mass spectroscopy signal intensities in AOX$^{-/-}$ mice than in wild-type untreated mice (6). These results also indicated that the protein profile of AOX$^{-/-}$ mice was similar to that of wild-type mice treated with Wy-14,643, a potent peroxisome proliferator, but significantly different from that of untreated wild-type mice. By liquid chromatography coupled with tandem mass spectrometry (LC–MS-MS) analysis, we identified one of the down-regulated peaks in AOX$^{-/-}$ mice as a major urinary protein (6).

As a continuation of that work and to further investigate the molecular mechanism of peroxisome proliferator-induced hepatocarcinogenesis, we used in this study the recently developed fluorescence two-dimensional differential in-gel electro-

* Corresponding author. Mailing address for Janardan K. Reddy: Department of Pathology, Feinberg School of Medicine, Northwestern University, 303 E. Chicago Ave., Chicago, IL 60611. Phone: (312) 503-8144. Fax: (312) 503-8249. E-mail: jkreddy@northwestern.edu. Mailing address for Ruiyin Chu: Department of Functional Genomics, Aventis Pharmaceuticals, Inc., P.O. Box 6800, Bridgewater, NJ 08807. Phone: (908) 231-4917. Fax: (908) 231-2707. E-mail: ruiyin.chu@aventis.com.

phoresis (2-D DIGE) technology (49) to compare the liver protein profile of AOX$^{-/-}$ mice with those of Wy-14,643-treated and untreated wild-type mice. Following trypsin protease digestion, differentially expressed protein spots were analyzed by LC–MS-MS to identify proteins (24). We report here the analysis of differential protein expression in AOX$^{-/-}$ and Wy-14,643-treated wild-type mice and the identification of 46 differentially expressed proteins. By gene ontology annotation (1, 51), these differentially expressed proteins were aligned according to their primary function. These observations establish the similarities in protein profiles in livers with PPARα activation by natural and synthetic ligands. Functionally, there is a preponderance of proteins involved in fatty acid metabolism in livers with PPARα activation, implying that higher PPARα activity contributes excess energy combustion.

MATERIALS AND METHODS

Animals. Wild-type (C57BL/6J) and AOX-null (AOX$^{-/-}$) male mice (10), 3 to 4 months of age, were housed in a controlled environment with a 12-h-light–12-h-dark cycle. They were provided with free access to water and standard laboratory chow. Wild-type mice were fed powdered chow containing Wy-14,643 (0.125%, wt/wt), a synthetic peroxisome proliferator, ad libitum for 2 weeks. Control (wild-type) mice received powdered chow with the solvent dimethyl sulfoxide and without Wy-14,643. All animals were sacrificed by terminal anesthesia after 2 weeks, and their liver tissues were removed, snap-frozen, and stored at −80°C. All animal procedures used in this study were reviewed and approved by the Institutional Review Board for Animal Research of Northwestern University.

Protein sample preparation. Individual mouse livers were thawed and homogenized in 5 ml of homogenization buffer (10 mM Tris-HCl [pH 7.4], 0.25 M sucrose, 1 mM EDTA, 1 mM phenylmethylsufonyl fluoride, 2.5 mg of aprotinin/ml, antipain, and leupeptin) on ice, with a Potter-type homogenizer using 15 strokes. Liver homogenates were pooled from three mice from each treatment group and centrifuged at 25,000 × *g* for 15 min, and the supernatants were collected. Protein concentrations for each treatment group were determined by using the BCA protein assay (Pierce Chemical Co., Rockford, Ill.), and the final concentration of the supernatant was adjusted to 20 mg/ml by adding the homogenization buffer. The protein samples were aliquoted and stored at −80°C before use.

2-D DIGE and image analysis. For two-dimensional gel analysis, the pooled samples were labeled by the DIGE fluorescent dyes as described elsewhere (49). Briefly, 300 μg of protein from each pooled sample was diluted to a final volume of 200 μl with labeling buffer containing 7 M urea, 2 M thiourea, and 4% CHAPS {3-[(3-cholamidopropyl)-dimethylammonio]-1-propanesulfonate} in 10 mM Tris-HCl (pH 9.0). Three cyanine dyes, Cy2, Cy3, and Cy5 (Amersham Biosciences, Piscataway, N.J.), were used to label the three treatment groups of liver protein samples (wild type, AOX$^{-/-}$, and Wy-14,643 treated, respectively) in a ratio of 50 μg of protein to 200 pmol of dye for 30 min. The reaction was terminated by the addition of 6 μl of 10 mM lysine, and the labeled proteins from the three treatment groups were then mixed together. For the first-dimension separation, the labeling mixture was applied to six Immobiline DryStrips (24 cm long, pHs 3 to 10; Amersham Biosciences) with a total of 120 kV · h of isoelectric focusing. The second dimension was carried out with six 10% SDS-PAGE gels, and gel images were subsequently acquired at the recommended wavelengths by using a 2920-2D Master Imager (Amersham Biosciences). Fluorescence Cy2, Cy3, and Cy5 DIGE images from three replicated gels with good separation quality were selected for comprehensive image analysis by using DeCyder differential in-gel analysis (DIA) and biological variation analysis (BVA) software programs (Amersham Biosciences). Statistical data were drawn from triplicate gels. Spots with a Student's *t* test *P* value of less than 0.05 and an average change greater than 1.5-fold were considered statistically significantly regulated spots. A proportion of these differentially expressed spots was further analyzed by LC–MS-MS to determine protein identification.

Protein identification by LC–MS-MS. For protein identification, two of the cyanine dye-labeled gels were subsequently stained with SYPRO Ruby fluorescent stain according to the manufacturer's protocol (Molecular Probes, Eugene, Oreg.). The SYPRO Ruby images were acquired by using the manufacturer's recommended wavelength and the 2920-2D Master Imager and were then positionally matched to the cyanine dye images with DeCyder BVA image analysis software. Selected differentially expressed spots identified from the DeCyder analysis of the cyanine DIGE images were excised from the 2-D gel with a Ettan spot picker (Amersham Biosciences) and processed for microliquid chromatography-electrospray ionization MS-MS analysis as described previously (6). The MS-MS spectra from an individual spot were used to search a mammalian subset of the NCBI nonredundant database with the SpectrumMill database search engine (Millennium Pharmaceuticals, Inc., Cambridge, Mass.). To obtain a functional annotation for the identified proteins, the coding sequence of each protein was searched with BLAST against sequences in the NCBI GenBank (Bethesda, Md.) database, and gene ontology information was then retrieved. The identified proteins were grouped according to their known or putative primary functions and ranked by the change in their level of expression (*n*-fold) in AOX$^{-/-}$ mice compared to their expression level in wild-type mice. When a protein was identified from multiple spots, the most significant increase (*n*-fold) among these spots was used. When two proteins were identified in the same spot, the same change (*n*-fold) was assigned to both proteins.

Western blot analysis. To confirm the 2-D DIGE results, mouse liver proteins were first separated in precast 4 to 20% Tris-glycine gels (Invitrogen, Carlsbad, Calif.) and then blotted onto polyvinylidene difluoride membranes. Following blocking with 4% nonfat milk, the membranes were probed sequentially with primary and secondary antibodies, and immunoreactive bands were detected with enhanced chemiluminescence substrate (Pierce Chemical Co.). Primary antibodies against mouse glutathione *S*-transferase P1 (GST-P1) and catalase were purchased from BioTrend Chemikalien GmbH (Cologne, Germany) and U.S. Biological (Swampscott, Mass.), respectively. Horseradish peroxidase-conjugated secondary antibodies were purchased from Santa Cruz Biotechnology, Inc. (Santa Cruz, Calif.).

RESULTS

2-D DIGE profile of mouse liver proteins. Total soluble liver proteins of wild-type, AOX$^{-/-}$, and Wy-14,643-treated mice were labeled with different fluorescent dyes and then mixed together and electrophoretically separated in the same 2-D gel. Figure 1 shows the Cy2, Cy3, and Cy5 images obtained from a representative 2-D DIGE gel, corresponding to wild-type, AOX$^{-/-}$, and Wy-14,643-treated mouse liver proteins, respectively. Protein spots were uniformly distributed across the 3- to 10-pI range in the first dimension and between 15 and 160 kDa in the 10% SDS-PAGE second dimension. An average of about 1,500 spots was detected in each image by DeCyder DIA image analysis, with pixel intensities ranging from 500 to 64,000 (data not shown). Differences in spot population and intensity were clearly visible among these three images, especially near the basic (pI 10) end.

2-D DIGE gel image analysis. One of the key advantages of 2-D DIGE technology is that fluorescent Cy2, Cy3, and Cy5 dyes used for protein labeling are matched by molecular weight and charge. Therefore, proteins with the same molecular weight and pI (i.e., the same protein) from different samples run on the same gel coelectrophoresce and migrate to the same position (i.e., the spots). Figure 2 shows positionally superimposed representative images of wild-type and AOX$^{-/-}$ mice, AOX$^{-/-}$ and Wy-14,643-treated mice, and wild-type and Wy-14,643-treated mice. Different colors show the different intensities of the matched spots. Blue, pink, and purple spots, corresponding to decreased expression, increased expression, and the same expression, respectively, were seen in all three overlaid images. A quantitative statistical analysis was performed by DeCyder BVA. The Venn diagram (Fig. 2D) summarizes the significantly regulated spots. One hundred sixty-four regulated spots were identified in the overlaid image of AOX$^{-/-}$ and wild-type mice, whereas only 68 regulated spots were identified for AOX$^{-/-}$ and Wy-14,643-treated mice. In contrast, 212 regulated spots were identified for Wy-14,643-treated and wild-

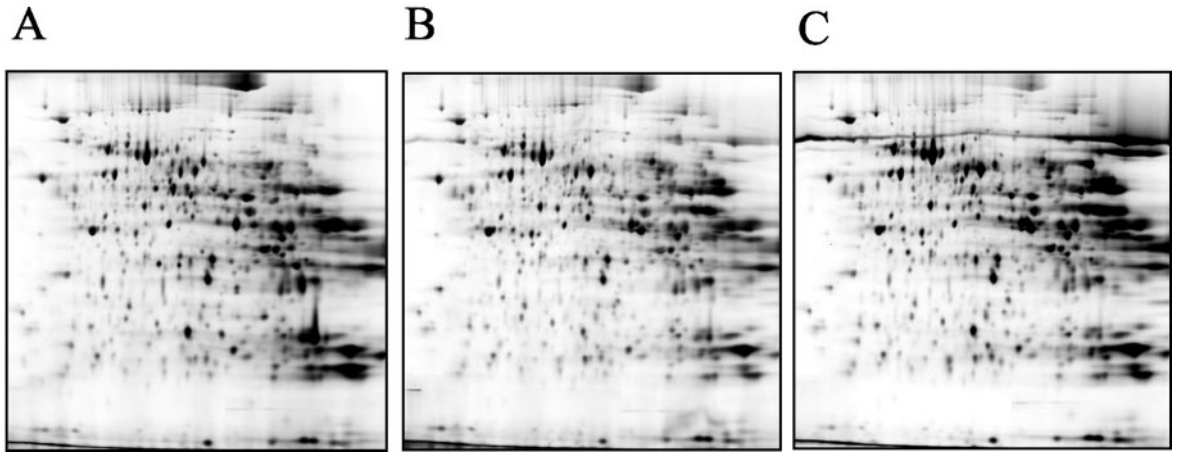

FIG. 1. Fluorescent cyanine dye images of mouse liver proteins. Proteins of three different mouse liver homogenates were labeled with cyanine dyes and mixed together for 2-D DIGE analysis. The mixture was first separated by isoelectric focusing (pH 3 to 10; horizontal axis) and further separated by 10% SDS-PAGE (vertical axis), which stretches from approximately 160 kDa (top) to 15 kDa (bottom). (A) Wild-type mouse liver protein labeled with Cy-2 dye; (B) AOX-null mouse liver protein labeled with Cy-3 dye; (C) liver protein of Wy-14,643-treated wild-type mouse labeled with Cy-5 dye.

type mice, the largest difference in this three-way comparison. In addition, six spots were found to be different in all three comparisons, as shown in the center of the Venn diagram.

Notably, there were three abundant spot clusters that showed the most dramatic changes among the treatment groups (Fig. 3). Each of these spot clusters consisted of three to six spots, as detected by DeCyder DIA. One spot from each cluster (master spot numbers 49, 268, and 386, as assigned by the DeCyder program) was selected, and its expression pattern was extracted from the DeCyder BVA results. As shown in the enlarged portion of the images, these three spots exhibited distinct patterns of change. The standardized log abundance chart indicated that spot 49 was moderately down-regulated in $AOX^{-/-}$ mice and further down-regulated in Wy-14,643-treated mice; spot 268, which had a very low level of expression in wild-type mice, was undetectable in $AOX^{-/-}$ mice but highly abundant in Wy-14,643-treated mice; spot 386, on the other hand, showed substantial up-regulation in $AOX^{-/-}$ mice and further up-regulation in Wy-14,643-treated mice. These three spots were subsequently identified as carbamoyl-phosphate synthetase I (Cpsase I) (molecular mass, 164 kDa; pI, 6.3 [spot 49]), AOX (molecular mass, 75 kDa; pI, 8.6 [spot 268]), and peroxisomal bifunctional enzyme (molecular mass 78 kDa; pI, 9.2 [spot 386]).

Protein identification. LC–MS-MS analysis of 56 SYPRO Ruby-stained 2-D DIGE gel spots generated a total of 57 protein identifications. Of 56 spots, 3 did not produce any protein identity, 4 were a mixture of two proteins, and 49 generated a single protein identification for each spot. Some proteins were identified from multiple spots. For example, farnesyl pyrophosphate synthase was identified from three spots. Similarly, fructose-1,6-bisphosphatase was identified from four spots (Fig. 4). Thus, there were 46 unique proteins among the 57 proteins identified.

Differentially expressed proteins. In order to assess functional relevance of changes in the identified proteins, the proteins were aligned into four groups according to their primary functions. The first group consisted of 12 proteins involved in fatty acid metabolism (Table 1). Nine of these 12 proteins were up-regulated in both $AOX^{-/-}$ and Wy-14,643-treated mice in comparison to levels in wild-type mice. Since fatty acid metabolism has been studied to a great extent in peroxisome proliferation, 7 of the 12 proteins, AOX (4, 25, 44, 51), medium-chain acyl-CoA dehydrogenase (7, 34), acyl-CoA thioesterase 1 (9, 47, 48), 3-hydroxy-3-methylglutaryl-CoA synthase 1 (45), 3-ketoacyl-CoA thiolase A (33, 44), acyl-CoA thioester hydrolase (2), and L-peroxisomal bifunctional enzyme (33, 37, 44), had previously been reported to be regulated in $AOX^{-/-}$ mice or regulated by peroxisome proliferator treatment due to PPARα activation. These gene products contain functional peroxisome proliferator response elements (PPRE) in the promoter region (8, 40, 41). Five other proteins, namely, acetyl-CoA acetyltransferase (acetoacetyl-CoA thiolase), short-chain 3-hydroxyacyl-CoA dehydrogenase (HCDH), 2-hydroxyphytanoyl-CoA lyase (HPCL), farnesyl pyrophosphate synthase, and carnitine *O*-octanoyltransferase, appeared to be novel findings in connection with peroxisome proliferation. It would be important to delineate whether the upstream promoter regions of these genes contain PPRE. The gene knockout target AOX was absent, as expected, in $AOX^{-/-}$ mice (10, 11) and increased 5.39-fold in Wy-14,643-treated mice compared to levels in control mice. Short-chain HCDH and HPCL, however, showed no ($<$1.5-fold) change in $AOX^{-/-}$ mice but decreased 1.81-fold and increased 3.34-fold, respectively, in Wy-14,643-treated mice.

The second group was a collection of proteins involved mainly in amino acid metabolism (Table 2). It consisted of 15 proteins, 10 of which were down-regulated, 3 of which were unchanged, and 2 of which were up-regulated in the $AOX^{-/-}$ mice compared to levels in wild-type mice. Levels of 6 of these 15 proteins were also significantly different between $AOX^{-/-}$ and Wy-14,643-treated mice, indicating the divergence of AOX gene disruption. Arginase 1 (liver type) (21), Cpsase I (21), fructose-1,6-bisphosphatase (22), mitochondrial aspartate aminotransferase (30), and NADP-dependent malic enzyme (19, 35) have previously been shown to be regulated in livers with peroxisome proliferation. For the 10 others, an association

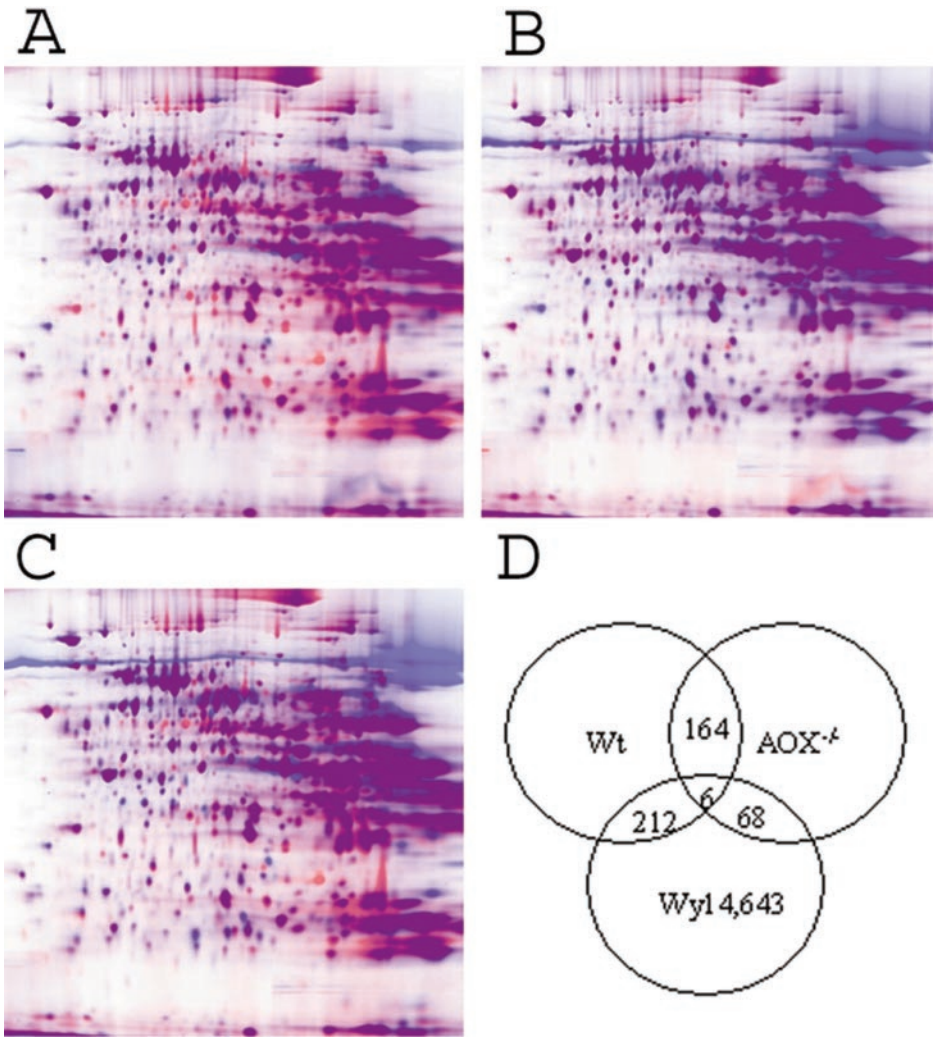

FIG. 2. Overlaid cyanine dye images and Venn diagram showing differential protein expression. Standard 24-bit 2-D DIGE gel images from Fig. 1 were overlaid one-to-one by Paint Shop. (A) Pink image of the wild-type mouse liver proteins overlaid with the blue image of $AOX^{-/-}$ mouse liver proteins. (B) Pink image of $AOX^{-/-}$ mouse liver proteins overlaid with the blue image of proteins from Wy-14,643-treated mice. (C) Pink image of proteins from wild-type mouse livers overlaid with the blue image of proteins from Wy-14,643-treated mice. Pink spots are more abundant in the first image; blue spots are more abundant in the second image, and purple spots have similar abundances in both images. (D) Venn diagram showing the number of 2-D gel spots with altered levels of expression between different mouse groups. The threshold used to qualify differentially expressed spots was a Student *t* test *P* value less than 0.05 and an average ratio of change greater than 1.5-fold. Wt, wild type.

with peroxisome proliferation had not been demonstrated previously. The up-regulation of NADP-dependent malic enzyme in Wy-14,643-treated mice appeared similar to that reported previously (19, 35). However, this regulation was not seen in the $AOX^{-/-}$ mice. Though the change in glutamate dehydrogenase expression in both $AOX^{-/-}$ and Wy-14,643-treated mice was not significant compared to its expression level in the wild-type mice, a 1.55-fold decrease was found in $AOX^{-/-}$ mice than in Wy-14,643-treated mice.

The third group consisted of proteins related to stress responses and xenobiotic metabolism (Table 3). Proteins in this group were all down-regulated in $AOX^{-/-}$ and Wy-14,643-treated mice, with the exception of HSP70 and catalase, both of which were up-regulated in $AOX^{-/-}$ and Wy-14,643-treated mice. Although catalase is not essential for the hypolipidemic action of peroxisome proliferators, it is the peroxisomal marker enzyme capable of degrading hydrogen peroxide generated by peroxisomal oxidases, including the AOX of the peroxisomal β-oxidation system (43). The sixfold increase of catalase protein in both $AOX^{-/-}$ and Wy-14,643-treated mice was significant. However, the regulation of catalase by PPARα has not been studied as extensively as that of fatty acid metabolism enzymes. A recent report provides evidence that a functional PPRE is present in the up-stream region of the rat catalase gene promoter and that catalase might be a PPARγ target gene (15). It should be noted that the catalase gene did not appear to be significantly transcriptionally up-regulated in livers with peroxisome proliferation (15, 44). The increase in the amount of the catalase protein in livers with PPARα activation is perhaps due to posttranscriptional regulations and not due to PPARα-regulated transcription. This issue requires further clarification by assessing the role of hydrogen

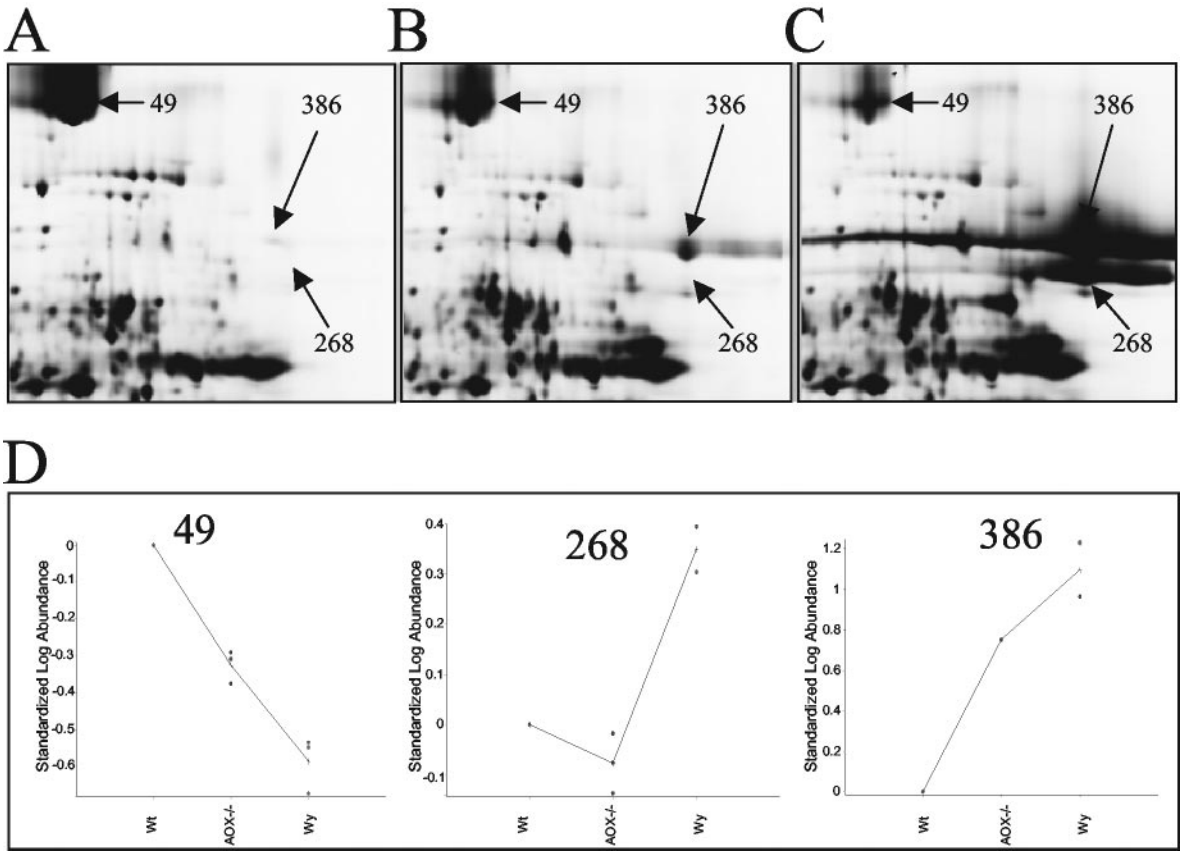

FIG. 3. Output from DeCyder BVA showing three differentially expressed abundant proteins. Top panels are enlarged regions of images of Cy2-labeled wild-type (A), Cy3-labeled AOX-null (B), and Cy5-labeled Wy-14,643-treated (C) mouse liver samples. Arrows indicate three abundant protein spots of 49, 268, and 386, corresponding to Cpsase I, AOX, and peroxisomal biofunctional enzyme, respectively. Bottom panels are graphical representations of standardized log abundances of these three protein spots exported from DeCyder BVA.

peroxide in the stability or posttranscriptional modification of catalase.

The final group included two carrier proteins and seven regulatory proteins responsible for protein modification and signal transduction (Table 4). Only an unknown protein with the putative function of tyrosine sulfation showed >7-fold down-regulation in both $AOX^{-/-}$ and Wy-14,643-treated mice than in the control mice. The other eight proteins exhibited moderate regulation, with less than a threefold change. Albumin was the only protein in this group that was known previously to be regulated by a peroxisome proliferator (24). All others have not been explored in association with peroxisome proliferation.

Confirmation of differential levels of protein expression by Western blotting. Among the significantly regulated proteins identified from 2-D DIGE gel spots by LC–MS-MS, some have been previously reported to be regulated at both the mRNA and protein levels in the livers of $AOX^{-/-}$ or peroxisome

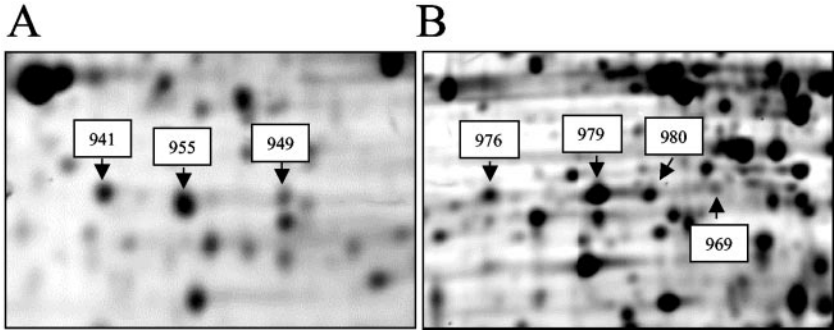

FIG. 4. Protein identification from multiple spots. Cyanine dye-labeled gels were further stained with SYPRO Ruby dye, and differentially expressed spots were excised and analyzed by LC–MS-MS. (A) Farnesyl pyrophosphate synthase was identified in spots 941, 949, and 955; (B) fructose-1,6-bisphosphatase was identified in spots 969, 976, 979, and 980.

TABLE 1. Fatty acid metabolism proteins[a]

GenBank accession no. (protein)	Protein description	Functions and pathways	AOX vs Wt		Wy vs AOX		Wy vs Wt	
			Fold	*P*	Fold	*P*	Fold	*P*
6429156	Peroxisomal AOX	Fatty acid β-oxidation, fatty acid metabolism, amino acid metabolism, energy derivation by oxidation of organic compounds	−1.13	0.39	6.11	0.26	5.39	0.00088
21431780	Short-chain HCDH	Fatty acid β-oxidation, fatty acid metabolism, energy pathways	1.03	0.57	−1.86	0.009	−1.81	0.037
9910332	HPCL	Fatty acid α-oxidation, carbohydrate metabolism, branched-chain family amino acid biosynthesis	1.19	0.2	2.8	0.044	3.34	0.021
135757	Acetyl-CoA acetyltransferase (acetoacetyl-CoA thiolase 1)	Fatty acid β-oxidation, lipid metabolism, ergosterol biosynthesis, nitrogen metabolism, energy pathways	1.50	0.00031	1.31	0.12	1.93	0.0073
15824695	Famesyl pyrophosphate synthase	Isoprenoid biosynthesis, modulator of the cellular response to fibroblast growth factor treatment	1.62	0.00027	1.41	0.018	2.28	0.00044
6680618 (mixture)	Medium-chain acyl-CoA dedydrogenase	Fatty acid β-oxidation, fatty acid metabolism, energy derivation by oxidation of organic compounds, energy pathways	1.91	0.000014	1.12	0.37	2.13	0.002
6753550 (mixture)	Acyl-CoA thioesterase 1	Fatty acid metabolism, bile acid metabolism, glycine metabolism	2.41	0.012	2.52	0.046	6.08	0.0068
8393538 (mixture)	3-Hydroxy-3-methylglutaryl-CoA synthase 1	Acetyl-CoA metabolism, cholesterol biosynthesis, lipid metabolism, steroid biosynthesis, coenzymes and prosthetic group metabolism	2.58	0.02	1.88	0.12	4.84	0.021
135746	3-Ketoacyl-CoA thiolase A	Fatty acid β-oxidation, lipid metabolism, ergosterol biosynthesis, nitrogen metabolism, energy pathways	2.83	0.05	−1.19	0.86	2.37	0.05
29336033	Carnitine *O*-octanoyltransferase	Fatty acid β-oxidation, fatty acid metabolism, synaptic transmission, energy derivation by oxidation of organic compounds, energy pathways	3.04	0.000058	−1.37	0.18	2.22	0.0047
12229867	Acyl-CoA thioester hydrolase 1	Fatty acid metabolism, bile acid metabolism, glycine metabolism	9.92	0.04	−1.11	0.84	8.93	0.03
16877282	Peroxisomal bifunctional enzyme	Fatty acid β-oxidation, fatty acid metabolism, energy pathways	14.21	0.037	1.87	0.099	26.54	0.025

[a] Fold, average ratio of change (*n*-fold). A positive number indicates an increase in the level of expression in the first mouse group or a decrease in the second mouse group; a negative number indicates a decrease in the level of expression in the first mouse group or an increase in the second mouse group. *P*, Student's *t* test *P* value; Wt, untreated wild-type mouse; AOX, AOX$^{-/-}$ mouse; Wy, wild-type mouse treated with Wy-14,643; mixture, two proteins identified from one spot.

proliferator-treated mice (10, 11). Other proteins, however, had not been reported before or showed a different trend of regulation. Catalase, for example, was previously shown to give a modest increase (approximately twofold) at the mRNA level but not at the protein level (11, 31). GST-π, on the other hand, was reported to be down-regulated in mice treated with different types of peroxisome proliferators (32, 50). To validate our 2-D DIGE results, we used immunoblotting with commercially available antibodies along with a more sensitive chemiluminescent substrate. As shown in Fig. 5, catalase-specific antibody detected a significant increase in the 60-kDa band, which is the expected molecular mass of catalase, in both AOX$^{-/-}$ and Wy-14,643-treated mice. GST-π-specific antibody, on the other hand, revealed the down-regulation of the band at 24 kDa, which is the anticipated molecular mass of GST-π, in both AOX$^{-/-}$ and Wy-14,643-treated groups. Intensity calculation of the detected bands indicated that the degrees of changes detected by immunoblotting were comparable to these detected with a 2-D DIGE gel (data not shown). In contrast, the control anti-β-tubulin antibody detected only a moderate decrease in the 50-kDa band, as expected.

DISCUSSION

This study applied 2-D DIGE technology to examine liver protein profiles of wild-type, AOX$^{-/-}$, and Wy-14,643-treated mice and identified 46 differentially expressed proteins by LC–MS-MS. The 2-D DIGE technology offers clear advantages over conventional 2-D gel methods, such as the capability of analyzing and comparing up to three different samples in one gel, good spot matching between images, and more accurate comparative analysis (49). On the other hand, 2-D DIGE bears some of the same limitations as traditional 2-D gel analysis. For example, membrane proteins and other low-abundance proteins are usually underrepresented. The recent cDNA microarray analysis identified several cell surface proteins which were substantially up-regulated in Wy-14,643-treated mouse liver (3, 26). None of these cell surface proteins, however, were detected in the present analysis, due to the ineffectiveness of the 2-D gel approach. Despite these limitations, proteomic analysis provides valuable information that is complementary to the genomic approach. It was shown in yeast that the mRNA level does not always correlate with the protein level (12, 17). To fully understand a biological process, it is necessary to determine the protein expression level directly. In addition, the proteomic approach provides information that could not be obtained at the RNA level. For instance, one mRNA may result in several isoforms of one protein with distinct biological functions. Of the 46 differentially expressed proteins identified in this study, six were found in multiple spots, implying the presence of multiple modified variants. On the other hand, changes in one protein may affect the functions of others.

TABLE 2. Amino acid metabolism proteins[a]

GenBank accession no. (protein)	Protein description	Functions and pathways	AOX vs Wt		Wy vs AOX		Wy vs Wt	
			Fold	*P*	Fold	*P*	Fold	*P*
15488638	Ketohexokinase	Monosaccharide metabolism, purine nucleotide metabolism, polysaccharide metabolism	−3.68	0.00017	1.35	0.11	−2.72	0.00078
16758338 (mixture)	Formiminotransferase-cyclodeaminase	Folic acid and glutamate metabolism, transport	−3.67	0.02	1.6	0.12	−2.29	0.021
114290	Arginosuccinate synthetase 1	Glutamine family amino acid biosynthesis, nitrogen metabolism, urea cycle intermediate metabolism	−2.63	0.0001	−1.01	0.93	−2.66	0.017
7106255	Arginase 1 (liver type)	Arginine metabolism, histidine metabolism, nitric oxide biosynthesis	−2.48	0.00049	1.15	0.13	−2.16	0.0047
15723268	Fructose-bisphosphatase aldolase B	Pyruvate kinase, glycolysis, fructose metabolism, catabolic carbohydrate metabolism	−2.17	0.0043	−1.14	0.31	−2.49	0.0037
8393186	Cpsase I	Arginine biosynthesis, de novo pyrimidine biosynthesis, nitrogen metabolism	−2.11	0.000022	−1.82	0.007	−3.85	0.00019
20149747	Scarcosine dehydrogenase	Glycine catabolism, glycerol-3-phosphate metabolism, small ubiquitin-related protein 1 conjugation, electron transport	−2.03	0.000053	−2.01	0.055	−4.07	0.024
20429722	Cysteine sulfinic acid decarboxylase	Histidine metabolism, catecholamine metabolism, glutamate decarboxylation, synaptic transmission	−1.81	0.00000073	1.15	0.13	−1.58	0.0026
9506589	Fructose-1,6-bisphosphatase	Amino acid and derivative metabolism, fructose metabolism, carbohydrate metabolism	−1.68	0.001	−1.3	0.15	−2.18	0.0043
1346309	4-Hydroxyphenylpyruvic acid dioxygenase	Tyrosine catabolism, apoptosis	−1.55	0.05	1.55	0.033	−1.01	NA[b]
6754036	Mitochondrial aspartate aminotransferase	Aspartate catabolism, glutamate metabolism, mitotic chromosome condensation	−1.24	0.0074	−1.36	0.15	−1.75	0.039
6678912	NADP-dependent malic enzyme	Malate metabolism, pyruvate metabolism, tricarboxylic acid cycle, carbohydrate metabolism	1.01	0.79	6.03	0.00002	6.11	0.002
6680027	Glutamate dehydrogenase, mitochondrial	Glutamate catabolism	1.35	0.00000016	−1.55	0.005	−1.16	0.14
8393215 (mixture)	Cystathionine gamma-lyase	Cysteine metabolism, methionine metabolism	1.91	0.0000014	1.12	0.37	2.13	0.002
15929766 (mixture)	*S*-Adenosylhomocysteine hydrolase	Methionine metabolism, DNA methylation	2.41	0.012	2.52	0.046	6.08	0.0068

[a] See the footnote for Table 1.
[b] NA, not available.

Accordingly, different proteins in the same or a related metabolic pathway may be regulated in a coordinated manner. Alignment of the differentially expressed proteins by their primary function indeed revealed similar patterns of changes.

Fatty acid metabolism. Peroxisomes are the principal sites of oxidation of long- and very long-chain fatty acids. More than half of the peroxisomal proteins participate in lipid metabolism (40, 41). Previously it has been shown that deletion of the AOX gene leads to sustained activation of PPAPα, resulting in profound spontaneous peroxisome proliferation in liver cells as well as induction of genes that are regulated by PPARα (10, 11). The observation of up-regulation of fatty acid metabolism proteins in $AOX^{-/-}$ mouse liver is consistent with the previous results. The magnitude of differential protein expression in $AOX^{-/-}$ mice is comparable with that of Wy-14,643-treated mice. Increases in proteins that function in fatty acid metabolism following disruption of the AOX gene, which produces one of the crucial enzymes in fatty acid catabolism, may be viewed simply as compensatory overexpression of the metabolic protein network. On the other hand, the loss of AOX leads to unmetabolized AOX substrates that function as ligands for PPARα (11, 52). Differences between $AOX^{-/-}$ and Wy-14,643-treated mice were limited to the short-chain HCDH and the α-oxidation enzyme HPCL (Table 1). The majority of these proteins are also related to energy pathways; some also participate in glycine metabolism (acyl-CoA thioesterase 1 and acyl-CoA thioester hydrolase), nitrogen metabolism (acetoacetyl-CoA thiolase), and steroid biosynthesis (3-hydroxy-3-methylglutaryl-CoA synthase 1).

Amino acid metabolism. Gene regulation studies of livers with peroxisome proliferation have been focused mostly on fatty acid-metabolizing enzymes. Most of the proteins involved in amino acid metabolism identified here have not been reported before to have direct connections with peroxisome proliferation. Unlike fatty acid metabolism proteins, the proteins in this group are mostly down-regulated in both $AOX^{-/-}$ and Wy-14,643-treated mice. Recently, it has been reported that PPARα influences the expression of numerous genes implicated in major pathways of amino acid metabolism (21). It was also demonstrated that the mRNA level of the Cpsase I gene was substantially decreased in Wy-14,643-treated wild-type mice (21). Suppression of its amino acid metabolism protein may result in an overall decrease in amino acid degradation. This speculation is supported by the fact that plasma urea concentrations are increased in fasted PPARα-null mice (21).

Stress response and xenobiotic metabolism. Oxidative stress and xenobiotic detoxification are physiologically correlated (29). A direct consequence of sustained induction of peroxisomal fatty acid β-oxidation system is the accumulation of excess H_2O_2 and possibly other reactive oxygen specials (16, 36, 52). Cells have numerous defense systems to counteract the deleterious effects of reactive oxygen specials. There are three

TABLE 3. Stress response and xenobiotic metabolism proteins[a]

GenBank accession no. (protein)	Protein description	Putative functions and pathways	AOX vs Wt		Wy vs AOX		Wy vs Wt	
			Fold	*P*	Fold	*P*	Fold	*P*
9507079	Selenium-binding protein 2 (56-kDa acetaminophen-binding protein)	Selenium and acetaminophen binding, detoxification	−18.62	0.0000017	−1.32	0.21	−24.54	0.0000021
10092608	GST-P1	Glutathione metabolism, glutathione conjugation reaction, prostaglandin metabolism, stress response	−8.28	0.00059	1.28	0.18	−6.48	0.0009
2494382	Liver carboxylesterase precursor (es-male) (esterase-31)	Acetylcholine breakdown in the synaptic cleft, cholesterol metabolism, membrane lipid metabolism, xenobiotic detoxification	−7.5	0.00026	3.37	0.31	−2.23	0.48
6754082	GST alpha 4	Glutathione metabolism, glutathione conjugation reaction, prostaglandin metabolism, stress response	−3.25	0.00032	1.01	0.99	−3.24	0.0012
127527	Major urinary protein 2 precursor	Prostaglandin metabolism, transport, defense response, olfaction	−3.16	0.0085	1.32	0.97	−4.17	0.0082
25108890	Sorbitol dehydrogenase	Sorbitol metabolism, ethanol oxidation	−3.1	0.00000049	3.1	0.00004	−1.01	0.94
6753036	Aldehyde dehydrogenase 2	Alcohol metabolism, aldehyde metabolism, vitamin A metabolism	−1.62	0.0021	1.05	0.69	−1.56	0.0047
3219774	Antioxidant protein 2 (1-Cys peroxiredoxin)	Electron transport, peroxidase reaction, oxidative-stress response, antiapoptosis	−1.61	0.0000013	−1.01	0.9	−1.63	0.005
14917005	Stress-70 protein (75-kDa glucose-regulated protein)	Heat shock response, protein folding, protein biosynthesis, translocation	2.28	0.0000022	−1.59	0.012	1.42	0.028
115704	Catalase	Catalase reaction, peroxidase reaction, oxidative-stress response	5.76	0.0000023	1.13	0.53	6.49	0.00026

[a] See the footnote for Table 1.

species of superoxide dismutases that transform the superoxide anion O_2^- in hydrogen peroxide. This transformed superoxide anion in turn is destroyed by peroxisomal catalase or by various peroxidases (19). It is not surprising to see an approximately sixfold increase of catalase protein in both $AOX^{-/-}$ and Wy-14,643-treated mice, despite the fact that only an approximately twofold increase of mRNA was observed (31, 44). The comparable ratios of catalase induction in $AOX^{-/-}$ and Wy-14,643-treated mice imply a common regulatory mechanism for catalase protein. Clearly, deletion of the AOX gene in $AOX^{-/-}$ mice prevents hydrogen peroxide production from acyl-CoA oxidation. If the increased expression of catalase in $AOX^{-/-}$ mice is in response to oxidative stress, a near-sixfold increase of catalase protein expression in the absence of AOX protein suggests the existence of additional reactive-oxygen-generating sources in $AOX^{-/-}$ mice that are independent of the peroxisomal fatty acid β-oxidation system. These additional sources are possibly attributable to a significant increase in the CYP4A family of enzymes in livers with PPARα activation (41, 52). In addition to catalase, GRP75, which is a stress protein, was increased only in $AOX^{-/-}$ mice, not in Wy-14,643-treated wild-type mice, implying a different stress response mechanism. Among eight down-regulated proteins, the most significantly changed protein was selenium-binding pro-

TABLE 4. Protein modification, signal transduction, and carrier proteins[a]

GenBank accession no. (protein)	Protein description	Putative function(s)	AOX vs Wt		Wy vs AOX		Wy vs Wt	
			Fold	*P*	Fold	*P*	Fold	*P*
15079395	Unknown (protein for RIKEN cDNA 493140)	Tyrosine sulfatation	−7.78	0.00022	1.11	0.56	−7.02	0.000000029
28526830	Secretory carrier membrane protein 1	Recycling carrier protein, endocytosis	−2.72	0.00072	1.12	0.87	−2.62	0.023
8567354	Glycine *N*-methyltransferase	Protein modification, ergosterol biosynthesis	2.7	0.0002	−1.11	0.38	−3	0.00011
5915682	Serum albumin precursor	Carrier/transporter	−2.13	0.000000005	2.6	0.004	1.19	0.31
12842842	Pyrophosphate phospho-hydrolase	Phosphate metabolism, cell cycle control	−1.59	0.0025	−1.13	0.38	−1.81	0.033
8394015	Protein phosphatase 1D magnesium-dependent delta isoform	Radiation response, protein dephosphorylation, cell cycle control, activation of p53, negative control of cell proliferation	−1.53	0.0021	1.31	0.061	−1.18	0.26
6679235 (mixture)	Phosphatidylcholine transfer protein	Protein phosphorylation	1.26	0.0025	1.62	0.051	2.04	0.017
548898 (mixture)	GTP-binding protein SAR1a	Intracellular protein traffic, protein myristylation, vesicle assembly, synaptic vesicle endocytosis	1.26	0.0025	1.62	0.051	2.04	0.017
12597249	RhoGDI-1	RHO protein signal transduction, cell adhesion inhibition, actin cytoskeleton reorganization, immune response, developmental processes	2.2	0.025	−1.65	0.19	1.33	0.33

[a] See the footnote for Table 1.

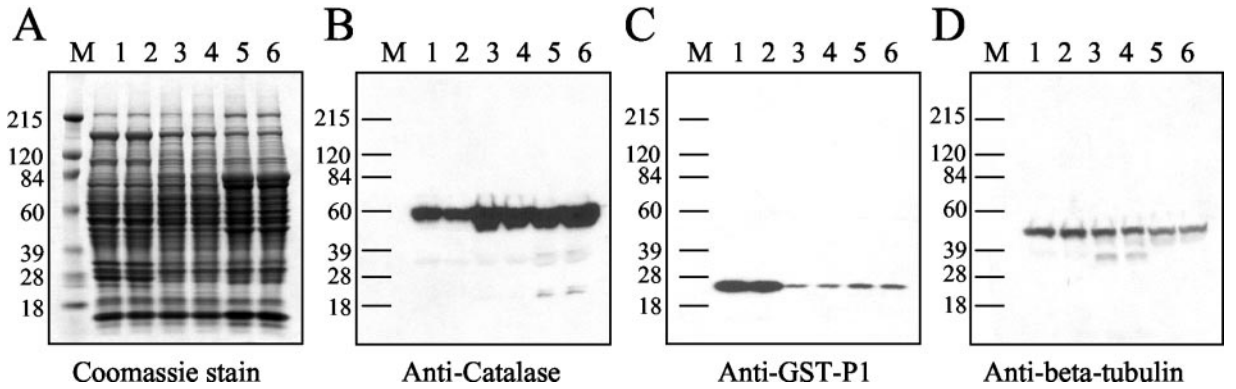

FIG. 5. Confirmation of differential protein expression by Western blotting. Liver protein samples (25 μg) from wild-type mice (lanes 1 and 2), AOX-null mice (lanes 3 and 4), and wild-type mice treated with Wy14,643 (lanes 5 and 6) were separated onto 4 to 20% SDS-PAGE gels, stained by Coomassie blue (A), or transferred to polyvinylidene difluoride membrane and probed with anticatalase antibodies (B), anti-GST-P1 antibodies (C), or anti-β-tubulin (D). After incubation with horseradish peroxidase-conjugated secondary antibody, signals were detected with an enhanced chemiluminescence substrate and recorded on X-ray films. Lanes M, molecular mass standards (in kilodaltons).

tein 2 (SBP2), which was reduced 18.6-fold in $AOX^{-/-}$ mice and 24.5-fold in Wy-14,643-treated mice. When a less sensitive Coomassie blue staining method was used for protein detection in the 2-D gel, SBP2 was reported to be down-regulated 9.6-fold in ciprofibrate-treated mice (13, 14). SPBs are believed to play a crucial role in the anticarcinogenic and growth inhibition functions of selenite by acting as growth regulatory proteins (28). Other proteins in this group, including GST-P1, liver carboxylesterase precursor (Esterase-31), GST α4, major urinary protein 2 precursor, aldehyde dehydrogenase 2, and antioxidant protein 2 (1-Cys peroxiredoxin), were all reduced significantly in both $AOX^{-/-}$ and Wy-14,643-treated mice. Overall, the regulation of stress response and xenobiotic metabolism proteins in $AOX^{-/-}$ mice was similar to that in the Wy-14,643-treated mice, implying that the xenobiotic effects of the endogenously accumulated long-chain fatty acid acyl-CoAs are similar to those of Wy-14,643.

Protein modification, signal transduction, and carrier proteins. Due to their regulatory nature, this group of proteins showed moderate changes in expression, with the exception of a protein of unknown function, which was down-regulated more than sevenfold in both $AOX^{-/-}$and Wy-14,643-treated mice. The full-length coding sequence for this protein has been registered several times in the NCBI GenBank database (accession no. BC011540, BC025213, AK088123, BC016078, and NM_133732). A gene ontology search suggested its role in tyrosine sulfation, yet this predicted function has to be confirmed experimentally. In contrast to metabolism proteins, these regulatory proteins may play pivotal roles in the initiation and progression of cell proliferation and subsequent carcinogenesis. For example, the protein phosphatase 1D magnesium-dependent delta isoform is known to be inducible by p53 and regulates cell proliferation (5). Rho GDI-1 interacts with Rho, Rac, and Cdc42, which are important regulators of the actin cytoskeleton, phospholipid metabolism, membrane trafficking, smooth muscle contraction, cell cycle progression, cell transformation, apoptosis, and transcriptional activation (23). For these regulatory proteins, even though the increases are not as great as those of proteins involved in metabolic pathways, these alterations can also contribute to peroxisome proliferator-induced carcinogenesis and add to the burden of oxidative stress (36, 46, 52). Induction of the oncogenes c-Ha-ras, c-*myc*, and jun by several peroxisome proliferators has been reported for rodent species (27). The roles of each these regulatory proteins in peroxisome proliferation need to be further determined. Nonetheless, this additional list of proteins responsible for protein modification and signal transduction may facilitate the understanding of peroxisome proliferation-associated hepatocarcinogenesis.

In summary, liver protein profiles of wild-type, $AOX^{-/-}$, and Wy-14,643-treated mice were analyzed and compared by 2-D DIGE and resulted in the identification of 46 differentially expressed proteins. Most of these differentially expressed proteins are metabolic enzymes; several are regulatory proteins. The alignment of these regulated proteins according to their primary function revealed that most of the fatty acid metabolism proteins are up-regulated but that the majority of proteins involved in amino acid metabolism, stress response, and xenobiotic metabolism are down-regulated. Some of the proteins identified have multiple functions and are involved in several metabolic pathways. Overall, the degrees of difference in protein expression between $AOX^{-/-}$ and wild-type mice were similar to those between wild-type and Wy-14,643-treated mice.

ACKNOWLEDGMENTS

We are grateful to Leigh Ann Gielbelhaus and Inna Dzhanibekova for their technical assistance. We thank Mike Tocci for managerial support and critical reading of the manuscript.

This work was supported in part by National Institutes of Health grant GM23750 (to J.K.R.) and by the Joseph L. Mayberry Endowment Fund.

REFERENCES

1. **Baker, P. G., C. A. Goble, S. Bechhofer, N. W. Paton, R. Stevens, and A. Brass.** 1999. An ontology for bioinformatics applications. Bioinformatics **15:**510–520.
2. **Broustas, C. G., L. K. Larkins, M. D. Uhler, and A. K. Hajra.** 1996. Molecular cloning and expression of cDNA encoding rat brain cytosolic acyl-coenzyme A thioester hydrolase. J. Biol. Chem. **271:**10470–10476.
3. **Cherkaoui-Malki, M., K. Meyer, W. Cao, N. Latruffe, A. V. Yeldandi, M. S. Rao, C. Bradfield, and J. K. Reddy.** 2001. Identification of novel peroxisome proliferator-activated receptor α (PPARα) target genes in mouse liver using cDNA microarray analysis. Gene Expr. **9:**291–304.
4. **Chevalier, S., N. Macdonald, R. Tonge, S. Rayner, R. Rowlinson, J. Shaw, J. Young, M. Davison, and R. A. Roberts.** 2000. Proteomic analysis of differential protein expression in primary hepatocytes induced by EGF, tumour

necrosis factor alpha or the peroxisome proliferator nafenopin. Eur. J. Biochem. **267:**4624–4634.
5. **Choi, J., E. Appella, and L. A. Donehower.** 2000. The structure and expression of the murine wildtype p53-induced phosphatase 1 (Wip1) gene. Genomics **64:**298–306.
6. **Chu, R., W. Zhang, H. Lim, A. V. Yeldandi, C. Herring, L. Brumfield, J. K. Reddy, and M. Davison.** 2002. Profiling of acyl-CoA oxidase-deficient and peroxisome proliferator Wy14,643-treated mouse liver protein by surface-enhanced laser desorption/ionization ProteinChip Biology System. Gene Expr. **10:**165–177.
7. **Cresci, S., L. D. Wright, J. A. Spratt, F. N. Briggs, and D. P. Kelly.** 1996. Activation of a novel metabolic gene regulatory pathway by chronic stimulation of skeletal muscle. Am. J. Physiol. **270:**C1413–C1420.
8. **Desvergne, B., and W. Wahli.** 1999. Peroxisome proliferator-activated receptors: nuclear control of metabolism. Endocr. Rev. **20:**649–688.
9. **Engberg, S. T., T. Aoyama, S. E. Alexson, T. Hashimoto, and L. T. Svensson.** 1997. Peroxisome proliferator-induced acyl-CoA thioesterase from rat liver cytosol: molecular cloning and functional expression in Chinese hamster ovary cells. Biochem. J. **323:**525–531.
10. **Fan, C. Y., J. Pan, J., R. Chu, D. Lee, K. D. Kluckman, N. Usuda, I. Singh, A. V. Yeldandi, M. S. Rao, N. Maeda, and J. K. Reddy.** 1996. Hepatocellular and hepatic peroxisomal alterations in mice with a disrupted peroxisomal fatty acyl-coenzyme A oxidase gene. J. Biol. Chem. **271:**24698–24710.
11. **Fan, C. Y., J. Pan, N. Usuda, A. V. Yeldandi, M. S. Rao, and J. K. Reddy.** 1998. Steatohepatitis, spontaneous peroxisome proliferation and liver tumors in mice lacking peroxisomal fatty acyl-CoA oxidase. Implications for peroxisome proliferator-activated receptor alpha natural ligand metabolism. J. Biol. Chem. **273:**15639–15645.
12. **Futcher, B., G. I. Latter, P. Monardo, C. S. McLaughlin, and J. I. A. Garrels.** 1999. A sampling of the yeast proteome. Mol. Cell. Biol. **19:**7357–7368.
13. **Giometti, C. S., X. Liang, S. L. Tollaksen, D. B. Wall, D. M. Lubman, V. Subbarao, and M. S. Rao.** 2000. Mouse liver selenium-binding protein decreased in abundance by peroxisome proliferators. Electrophoresis **21:**2162–2169.
14. **Giometti, C. S., S. L. Tollaksen, X. Liang, and M. L. Cunningham.** 1998. A comparison of liver protein changes in mice and hamsters treated with the peroxisome proliferator Wy-14,643. Electrophoresis **19:**2498–24505.
15. **Girnun, G. D., F. E. Domann, S. A. Moore, and M. E. Robbins.** 2002. Identification of a functional peroxisome proliferator-activated receptor response element in the rat catalase promoter. Mol. Endocrinol. **16:**2793–2801.
16. **Gonzalez, F. J., J. M. Peters, and R. C. Cattley.** 1998. Mechanism of action of the nongenotoxic peroxisome proliferators: role of the peroxisome proliferator-activator receptor alpha. J. Natl. Cancer Inst. **90:**1702–1709.
17. **Gygi, S. P., Y. Rochon, B. R. Franza, and R. Aebersold.** 1999. Correlation between protein and mRNA abundance in yeast. Mol. Cell. Biol. **19:**1720–1730.
18. **Hashimoto, T., T. Fujita, M. Usuda, W. Cook, C. Qi, J. M. Peters, F. J. Gonzalez, A. V. Yeldandi, M. S. Rao, and J. K. Reddy.** 1999. Peroxisomal and mitochondrial fatty acid beta-oxidation in mice nullizygous for both peroxisome proliferator-activated receptor alpha and peroxisomal fatty acyl-CoA oxidase: genotype correlation with fatty liver phenotype. J. Biol. Chem. **274:**19228–19236.
19. **Hertz, R., V. Nikodem, A. Ben-Ishai, I. Berman, and J. Bar-Tana.** 1996. Thyromimetic mode of action of peroxisome proliferators: activation of 'malic' enzyme gene transcription. Biochem. J. **319:**241–248.
20. **Issemann, I., and S. Green.** 1990. Activation of a member of the steroid hormone receptor superfamily by peroxisome proliferators. Nature **347:**645–650.
21. **Kersten, S., S. Mandard, P. Escher, F. J. Gonzalez, S. Tafuri, B. Desvergne, and W. Wahli.** 2001. The peroxisome proliferator-activated receptor alpha regulates amino acid metabolism. FASEB J. **15:**1971–1978.
22. **Laybutt, D. R., A. Sharma, D. C. Sgroi, J. Gaudet, S. Bonner-Weir, and G. C. Weir.** 2002. Genetic regulation of metabolic pathways in β-cells disrupted by hyperglycemia. J. Biol. Chem. **277:**10912–10921.
23. **Lian, L. Y., I. Barsukov, A. P. Golovanov, D. I. Hawkins, R. Badii, K. H. Sze, N. H. Keep, G. M. Bokoch, and G. C. Roberts.** 2000. Mapping the binding site for the GTP-binding protein Rac-1 on its inhibitor RhoGDI-1. Structure Fold Des. **8:**47–55.
24. **Lim, H., J. Eng, J. R. Yates, S. L. Tollaksen, C. S. Giometti, J. F. Holden, M. W. Adams, C. I. Reich, G. J. Olsen, and L. G. Hays.** 2003. Identification of 2D-gel proteins: a comparison of MALDI/TOF peptide mass mapping to μ LC-ESI tandem mass spectrometry. J. Am. Soc. Mass Spectrom. **14:**957–970.
25. **Macdonald, N., S. Chevalier, R. Tonge, M. Davison, R. Rowlinson, J. Young, S. Rayner, and R. Roberts.** 2001. Quantitative proteomic analysis of mouse liver response to the peroxisome proliferator diethylhexylphthalate (DEHP). Arch. Toxicol. **75:**415–424.
26. **Meyer, K., J. S. Lee, P. A. Dyck, W. Q. Cao, M. S. Rao, S. S. Thorgeirsson, and J. K. Reddy.** 2003. Molecular profiling of hepatocellular carcinomas developing spontaneously in acyl-CoA oxidase deficient mice: comparison with liver tumors induced in wild-type mice by a peroxisome proliferator and a genotoxic carcinogen. Carcinogenesis **24:**975–984.
27. **Miller, R. T., S. E. Glover, W. S. Stewart, J. C. Corton, J. A. Popp, and R. C. Cattley.** 1996. Effect on the expression of c-met, c-myc and PPAR-alpha in liver and liver tumors from rats chronically exposed to the hepatocarcinogenic peroxisome proliferator WY-14,643. Carcinogenesis **17:**1337–1341.
28. **Milner, J. A.** 1986. Inhibition of chemical carcinogenesis and tumorigenesis by selenium. Adv. Exp. Med. Biol. **206:**449–463.
29. **Morel, Y., and R. Barouki.** 1999. Repression of gene expression by oxidative stress. Biochem. J. **342:**481–496.
30. **Motojima, K., P. Passilly, J. M. Peters, F. J. Gonzalez, and N. Latruffe.** 1998. Expression of putative fatty acid transporter genes are regulated by peroxisome proliferator-activated receptor alpha and gamma activators in a tissue- and inducer-specific manner. J. Biol. Chem. **273:**16710–16714.
31. **Nemali, M. R., N. Usuda, M. K. Reddy, K. Oyasu, T. Hashimoto, T. Osumi, M. S. Rao, and J. K. Reddy.** 1998. Comparison of constitutive and inducible levels of expression of peroxisomal beta-oxidation and catalase genes in liver and extrahepatic tissues of rat. Cancer Res. **48:**5316–5324.
32. **O'Brien, M. L., M. L. Cunningham, B. T. Spear, and H. P. Glauert.** 2001. Effects of peroxisome proliferators on glutathione and glutathione-related enzymes in rats and hamsters. Toxicol. Appl. Pharmacol. **171:**27–37.
33. **Osumi, T.** 1993. Structure and expression of the genes encoding peroxisomal beta-oxidation enzymes. Biochimie **75:**243–250.
34. **Ouali, F., F. Djouadi, C. Merlet-Benichou, and J. Bastin.** 1998. Dietary lipids regulate beta-oxidation enzyme gene expression in the developing rat kidney. Am. J. Physiol. **275:**F777–F784.
35. **Rao, K. N., M. S. Elm, R. H. Kelly, N. Chandar, E. P. Brady, B. Rao, H. Shinozuka, and P. K. Eagon.** 1997. Hepatic hyperplasia and cancer in rats: metabolic alterations associated with cell growth. Gastroenterology **113:**238–248.
36. **Rao, M. S., and J. K. Reddy.** 1987. Peroxisome proliferation and hepatocarcinogenesis. Carcinogenesis **8:**631–636.
37. **Rao, M. S., and J. K. Reddy.** 1996. Hepatocarcinogenesis of peroxisome proliferators. Ann. N. Y. Acad. Sci. **804:**573–587.
38. **Rao, M. S., H. Ide, A. V. Yeldandi, S. Kumar, and J. K. Reddy.** 1994. Expression of peroxisomal enoyl-CoA hydratase/3-hydroxyacyl-CoA dehydrogenase enzyme and its mRNA in peroxisome proliferator-induced liver tumors. Carcinogenesis **15:**2619–2622.
39. **Reddy, J. K.** 2004. Rous-Whipple Award Lecture. Peroxisome proliferators and peroxisome proliferator-activated receptor biotic and xenobiotic sensing. Am. J. Pathol. **164:**2305–2321.
40. **Reddy, J. K., and R. Chu.** 1996. Peroxisome proliferator-induced pleiotropic responses: pursuit of a phenomenon. Ann. N. Y. Acad. Sci. **804:**176–201.
41. **Reddy, J. K., and T. Hashimoto.** 2001. Peroxisomal β-oxidation and peroxisome proliferator-activated receptor α: an adaptive metabolic system. Annu. Rev. Nutr. **21:**193–230.
42. **Reddy, J. K., D. L. Azarnoff, and C. E. Hignite.** 1980. Hypolipidaemic hepatic peroxisome proliferators form a novel class of chemical carcinogens. Nature **283:**397–398.
43. **Reddy, J. K., S. K. Goel, M. R. Nemali, J. J. Carrino, T. G. Laffler, M. K. Reddy, S. J. Sperbeck, T. Osumi, T. Hashimoto, and N. D. Lalwani.** 1986. Transcription regulation of peroxisomal fatty acyl-CoA oxidase and enoyl-CoA hydratase/3-hydroxyacyl-CoA dehydrogenase in rat liver by peroxisome proliferators. Proc. Natl. Acad. Sci. USA **83:**1747–1751.
44. **Reddy, J. K., D. E. Moody, D. L. Azarnoff, and M. S. Rao.** 1997. Hepatic catalase is not essential for the hypolipidemic action of peroxisome proliferators. Proc. Soc. Exp. Biol. Med. **154:**483–487.
45. **Rodriguez, J. C., G. Gil-Gomez, F. G. Hegardt, and D. Haro.** 1994. Peroxisome proliferator-activated receptor mediates induction of the mitochondrial 3-hydroxy-3-methylglutaryl-CoA synthase gene by fatty acids. J. Biol. Chem. **269:**18767–18772.
46. **Rusyn, I., S. Asakura, B. Pachkowski, B. U. Bradford, M. F. Denissenko, J. M. Peters, S. M. Holland, J. K. Reddy, M. L. Cunningham, and J. A. Swenberg.** 2004. Expression of base excision DNA repair genes is a sensitive biomarker for in vivo detection of chemical-induced chronic oxidative stress: identification of the molecular source of radicals responsible for DNA damage by peroxisome proliferators. Cancer Res. **64:**1050–1057.
47. **Svensson, L. T., S. T. Engberg, T. Aoyama, N. Usuda, S. E. Alexson, and T. Hashimoto.** 1998. Molecular cloning and characterization of a mitochondrial peroxisome proliferator-induced acyl-CoA thioesterase from rat liver. Biochem. J. **329:**601–608.
48. **Svensson, L. T., M. Wilcke, and S. E. Alexson.** 1995. Peroxisome proliferators differentially regulate long-chain acyl-CoA thioesterases in rat liver. Eur. J. Biochem. **230:**813–820.
49. **Tonge, R., J. Shaw, B. Middleton, R. Rowlinson, S. Rayner, J. Young, F. Pognan, E. Hawkins, I. Currie, and M. Davison.** 2001. Validation and development of fluorescence two-dimensional differential gel electrophoresis proteomics technology. Proteomics **1:**377–396.
50. **Voskoboinik, I., R. Drew, and J. T. Ahokas.** 1996. Differential effect of peroxisome proliferators on rat glutathione *S*-transferase isoenzymes. Toxicol. Lett. **87:**147–155.
51. **Xie, H., A. Wasserman, Z. Levine, A. Novik, V. Grebinskiy, A. Shoshan, and L. Mintz.** 2002. Large-scale protein annotation through gene ontology. Genome Res. **12:**785–794.
52. **Yeldandi, A. V., M. S. Rao, and J. K. Reddy.** 2000. Hydrogen peroxide generation in peroxisome proliferator-induced oncogenesis. Mutat. Res. **448:**159–177.